DOR: 20.1001.1.27170314.2022.11.2.7.5

Research Paper

Feasibility Investigation of Hydroforming of Dental Drill Body by FEM Simulation

Mohammad Sajjad Mahdieh[1*], Mohammad Reza Esteki[2]
[1]Department of Mechanical Engineering, Shahid Chamran University of Ahvaz, Ahvaz, Iran
[2]Department of Mechanical Engineering, Foolad Institute of Technology, Isfahan, Iran
[*]Email of the Corresponding Author: s.mahdieh@scu.ac.ir
Received: June 13, 2022; Accepted: August 1, 2022

Abstract
Applying numerical methods in the analysis of forming processes, results in the prediction of the process parameters without performing costly and time-consuming laboratory test procedures. The purpose of this study is to evaluate the feasibility of manufacturing a dental drill body using a hydroforming process. Due to the hygienic issues, the selected material for this part is stainless steel grade 304. The main reason for applying stainless steel in the main body is its hygienic characteristics such as antibacterial surface and washability which makes it appropriate for use in many medical instruments. The hydroforming process is simulated in ABAQUS software and the required parameters of the initial material are obtained from engineering tables. The thickness of the initial part is 0.5 mm and after simulation, it is decreased to 0.38mm. The maximum Von Misses stress of the part reached in this simulation is 708 MPa and the maximum strain rate is 1.233 mm/mm.

Keywords
Stainless Steel, FEM Simulation, ABAQUS Software, Tube Hydroforming Process

1. Introduction

The manufacturing of dental drills is one of the concerns of medical industries in our country. A dental drill consists of several parts such as a turbine, bearings, gearbox, clutch, drive shaft, neck, and body (Figure 1). The dental drill is driven by a pneumatic system in which air pressure rotates a tiny motor and then the drill bit is rotated consequently.

Figure 1. Dental drill' parts [1]

The main body of the dental drill is made of stainless steel grades 301, 302, 304, and 316. The main reason for applying stainless steel in the main body is its hygienic characteristics such as antibacterial surface and washability which makes it appropriate for use in many medical instruments. Due to hygienic issues, washability, and strength of the main body of the dental drill, it should be made in one piece without any welding seam or spots. Therefore, a suitable manufacturing process in which the main body can be produced in one piece is hydroforming. Applying pressurized fluids in forming tubes and sheet metals has been conventional since the 1980s[2]. During the hydroforming of tubes, the axial forces are exerted as well and help the forming process[3, 4]. Without the axial feed, the

thickness of the tube's walls is dramatically reduced resulting in appear of cracks and raptures[5]. The schematic of the tube-hydroforming process is shown in Figure 2. After the hydroforming process, it is not necessary to use finishing processes such as grinding, vibratory finishing, burnishing, and barrel finishing [6-9]. In the mass production scale, the hydroforming process is more efficient and beneficial than other manufacturing methods such as machining, non-traditional machining, and sheet metal processes [10-15].

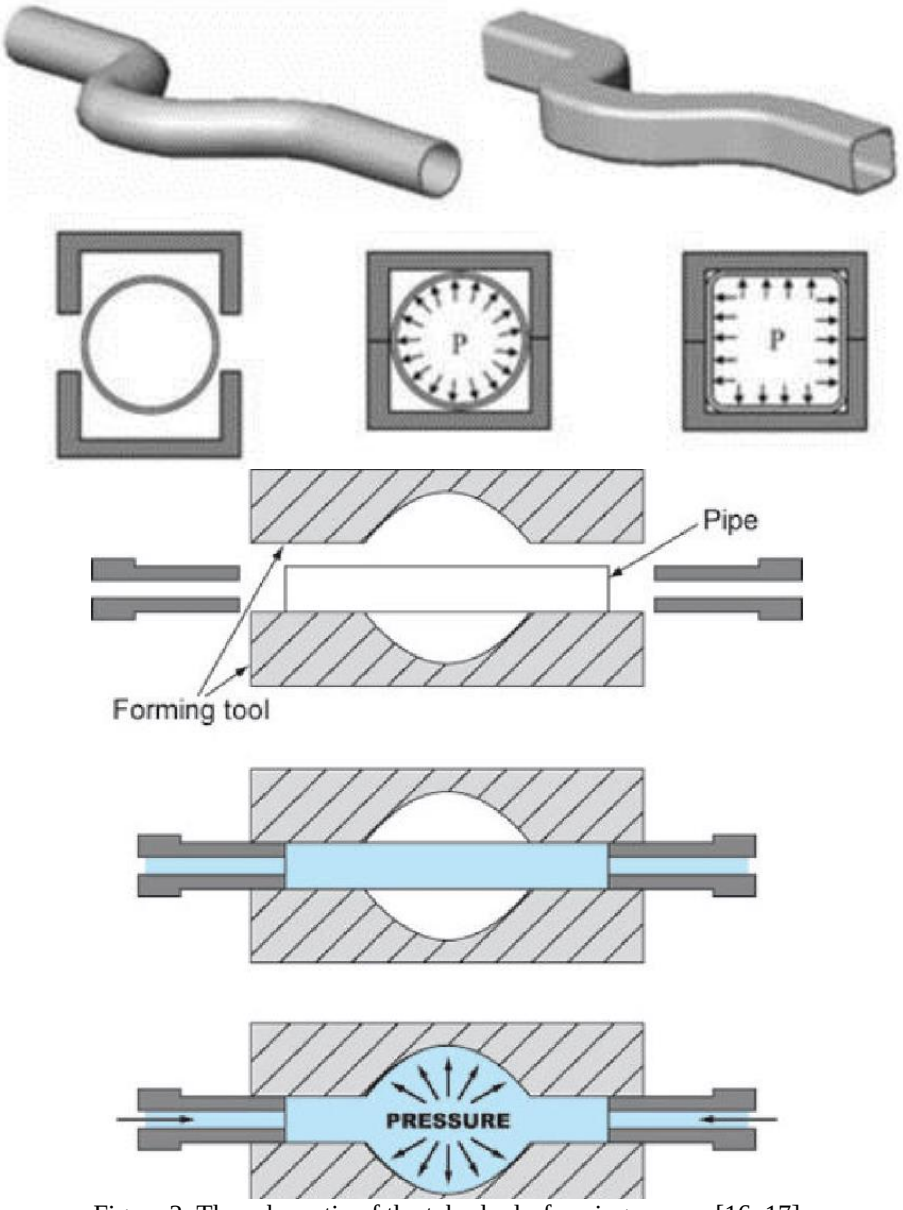

Figure 2. The schematic of the tube-hydroforming process[16, 17]

The pressure of the hydroforming process depends on the thickness of the tube, the mechanical properties of the metal, and the percentage of shaping[18, 19]. The advantages of hydroforming are the ability to form complicated geometry in one stage, higher precision, lower spring back, reduction in residual stress, and lower waste materials[20, 21]. Therefore, in recent years, the application of this process has increased in several industries such as the automotive industry, medical industry, oil

refinery industry, and defense industry [22, 23]. Figure 3 demonstrated some parts which are manufactured with a tube-hydroforming process.

Figure 3. Hydroforming products[24-26]

Desu et al. [27] worked on the mechanical properties of Austenitic Stainless Steel grade 304L and 316L at high temperatures. In their study, the mechanical properties such as ultimate tensile strength (UTS), yield strength (YS), % elongation, strain hardening exponent (n), and strength coefficient (K) are evaluated based on the experimental data obtained from the uniaxial isothermal tensile tests performed at an interval of 50 °C from 50 °C to 650 °C. Gheisary et al. [28] establish a basic understanding of the double bulge tube hydroforming process of stainless steel deep-drawn cups. Their method was briefly reviewed by carrying out experimental tests and Finite element analysis. Hwang et al. [29] used the finite element method to explore the plastic flow pattern of a circular tube that is hydraulically expanded or crushed into a rectangular cross-section. The tubes used in the crushing process have a larger diameter and are thinner than the tubes used in the hydraulic expansion test. The loading path and the forming procedures during the crushing process are discussed. Hwang et al. [30] evaluated the quality of the tubes produced by bulge hydroforming processes. In their study, a mathematical model by an ellipsoidal surface examined the plastic deformation behavior of a thin-walled tube during the bulge hydroforming process in an open die. Kashani et al. [31] simulated tube hydroforming of unequal T joints with the finite element method. They used ABAQUS in their study and they investigated the effects of the coefficient of friction, strain hardening exponent, and fillet radius on the parameters and thickness distribution of the process. Khorsandi et al [32] studied the hydroforming process of bent tubes in T-shaped die for pulsating and linear pressure paths by the finite element method. They used Forming Limit Diagrams (FLDs) and thickness distribution curves to investigate the effect of pulsating pressure on the hydroforming process. Choi et al. [33] made a comparison of an implicit and an explicit finite-element method which is widely used for the hydroforming process. Their comparisons focus on the accuracy of the predicted geometrical shape

and the stress in the explicit method with various scaling factors. Bakhshi et al. [34] investigated the pulsating hydroforming of a tube with a box die which was simulated by the finite element method to examine the effect of pulsating pressure on the improvement of formability. Then, they compared the calculated results with experimental results in which the improvement of the formability occurred before contact of the tube and die in the expansion zone of the tube. Mohammadalizade et al. [35] investigated the effects of internal pressure and axial feeding paths to improve the thickness distribution of stepped cylindrical tubes. They studied the constant pressure loading paths with various pressure levels, then, they investigated the pressure levels in which the parts weren't burst and formed perfectly.

In this paper, the feasibility of manufacturing the dental drill body by hydroforming process is investigated via FEM simulation. To obtain the hydroforming parameters including fluid pressure, material thickness reduction, and the maximum stress and strain, the process is simulated by ABAQUS software and then the maximum tensile stress, thickness reduction, formability, and appearance of cracks and rapture are obtained through these simulations.

2. Materials and methods

In this study, the simulations are performed in ABAQUS software version 2019. The initial model is designed via Inventor software version 2020. Figure 4 shows the initial part and the final part (using as mold) which are created in Inventor.

Figure 4. The initial part and the final part (used as mold) were created by Inventor

These models were then imported into ABAQUS software. The initial part imported in the Part module is 3D and formable and on the other hand, the die is solid and non-formable. The initial part and the die at the ABAQUS software are shown in Figure 5.

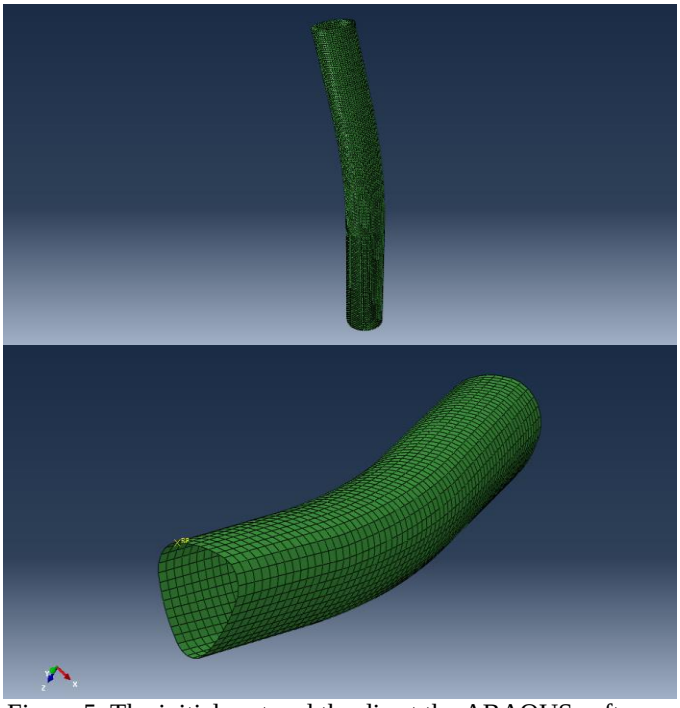

Figure 5. The initial part and the die at the ABAQUS software

In this project, the 304 stainless steel alloy which is very common in hygienic applications, is applied. The mechanical properties of this steel used in the Property module of ABAQUS are introduced in table 1. In addition, the σ-ε curves of 304 stainless steel in different temperatures are shown in Figure 6.

Table 1. The mechanical properties of 304 stainless steel

Type	E% in 50.8mm	YS(Mpa)	UTS (MPa)	Hardness (Rockwell B)
304	55(8.26%)	290	621	B82

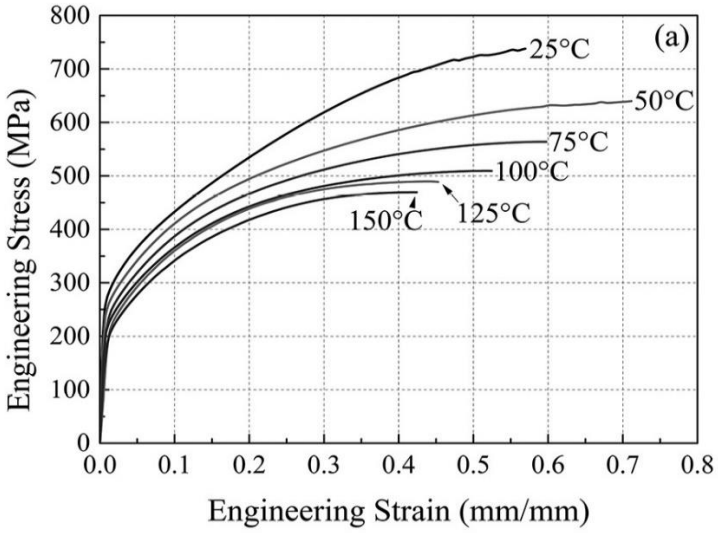

Figure 6. σ-ε curves of 304 stainless steel

The assembly of the die and initial part is performed in the Assembly module which is shown in Figure 7.

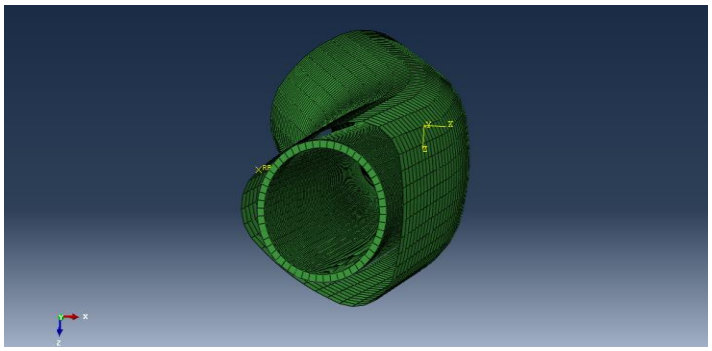

Figure 7. Assembly of the die and initial part in the Assembly module

The Dynamic Implicit solver is selected at the Step module to solve the problem and perform the simulation. In the Interaction module, general contact is defined to match the related points of the part and die. The oil film with a 0.15 friction coefficient is applied for lubricating. In the Load module, the surface force equal to 25kN is imposed on the internal surface of the part as shown in Figure 8. The degree of freedom of the die is zero and it is completely constrained.

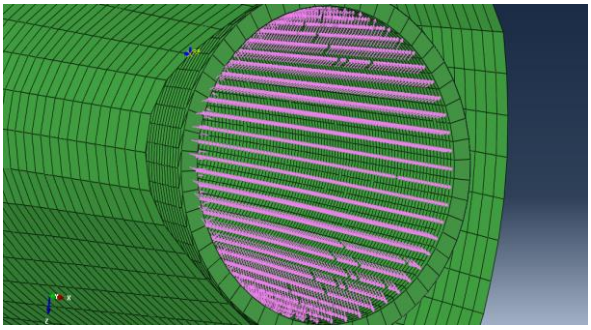

Figure 8. The pressure imposed on the internal surface of the part

In the Mesh module, the 0.2mm mesh size and the hexahedrons 8-nodes (C3D8R) mesh type is selected. After increasing the number of mesh elements up to 16592 elements, the results of the simulations are converged. Table 2 shows the alternation of maximum stress by increasing the number of mesh.

Table 2. Alternation of maximum stress by increasing the number of mesh

Number of mesh elements	The maximum stress in the part (MPa)
1188	740.1
1738	735
2646	728
4810	715.7
7335	710.5
10530	708.7
16592	708

3. Results and discussion

3.1 Stress and strain

The final shape of the part is shown in Figure 9. According to Figure 9, by applying the specified internal pressure, the final shape of the part is compatible with the die geometry and it shows that the simulation parameters have been adjusted properly.

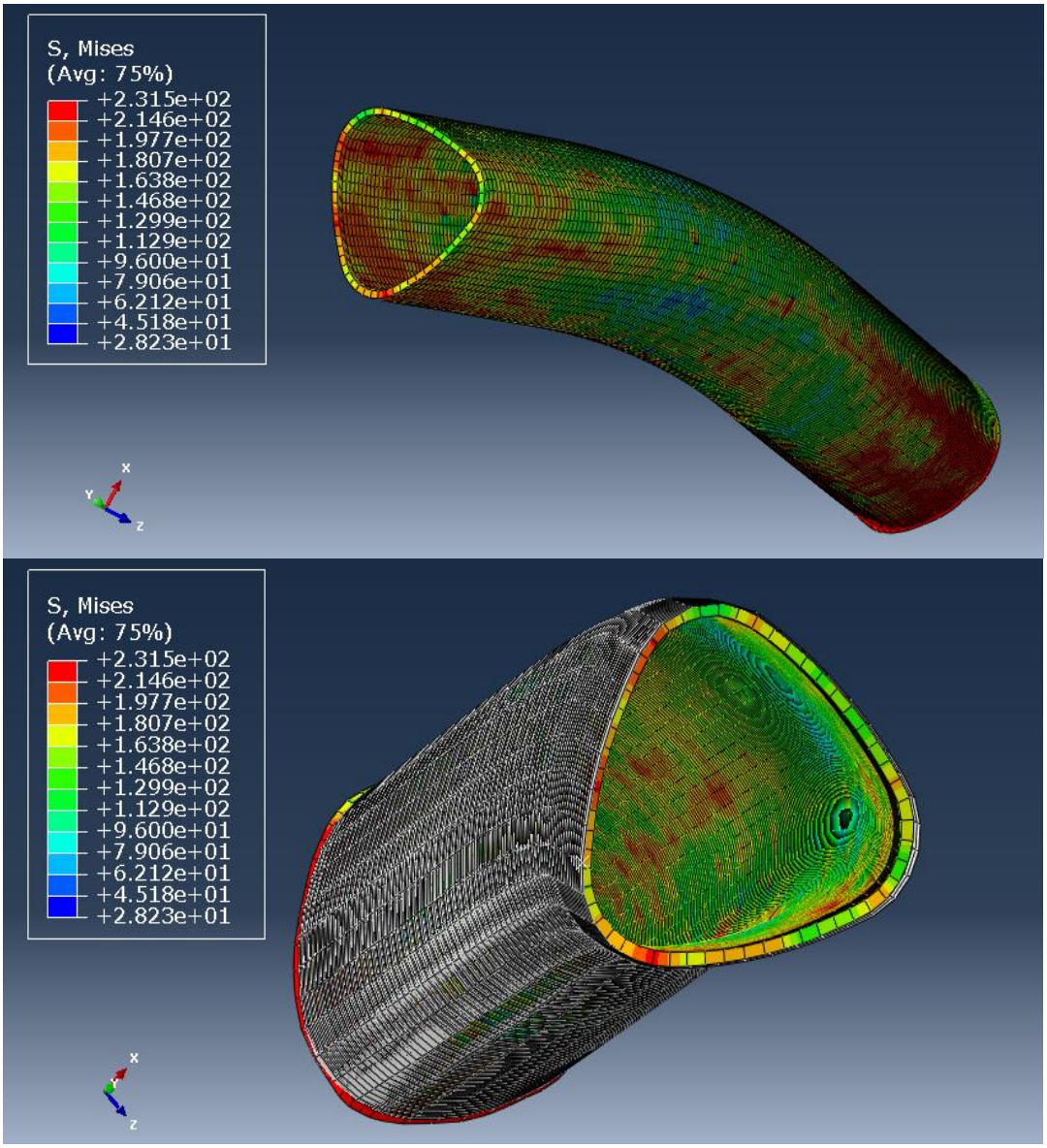

Figure 9. The final shape of the part

Figure 10 shows the steps of forming the simulation. It is obvious that the forming process has not started before yielding strength and when the internal pressure increases until reaches the yield strength, the forming process starts.

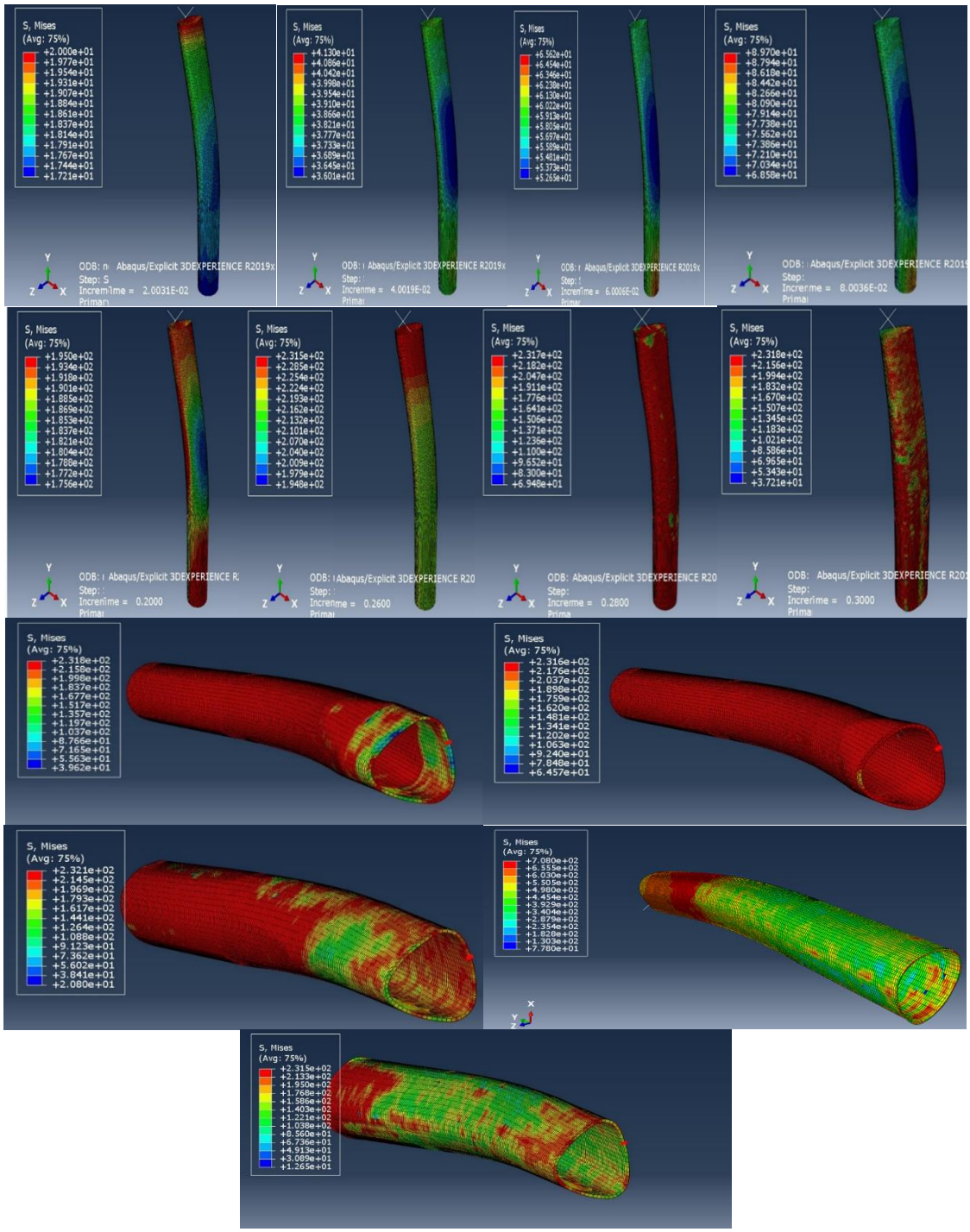

Figure 10. Steps of forming simulation

The maximum Von Misses stress that occurred in this simulation is equal to 708MPa and the position of the maximum and minimum stress contour is demonstrated in Figure 11.

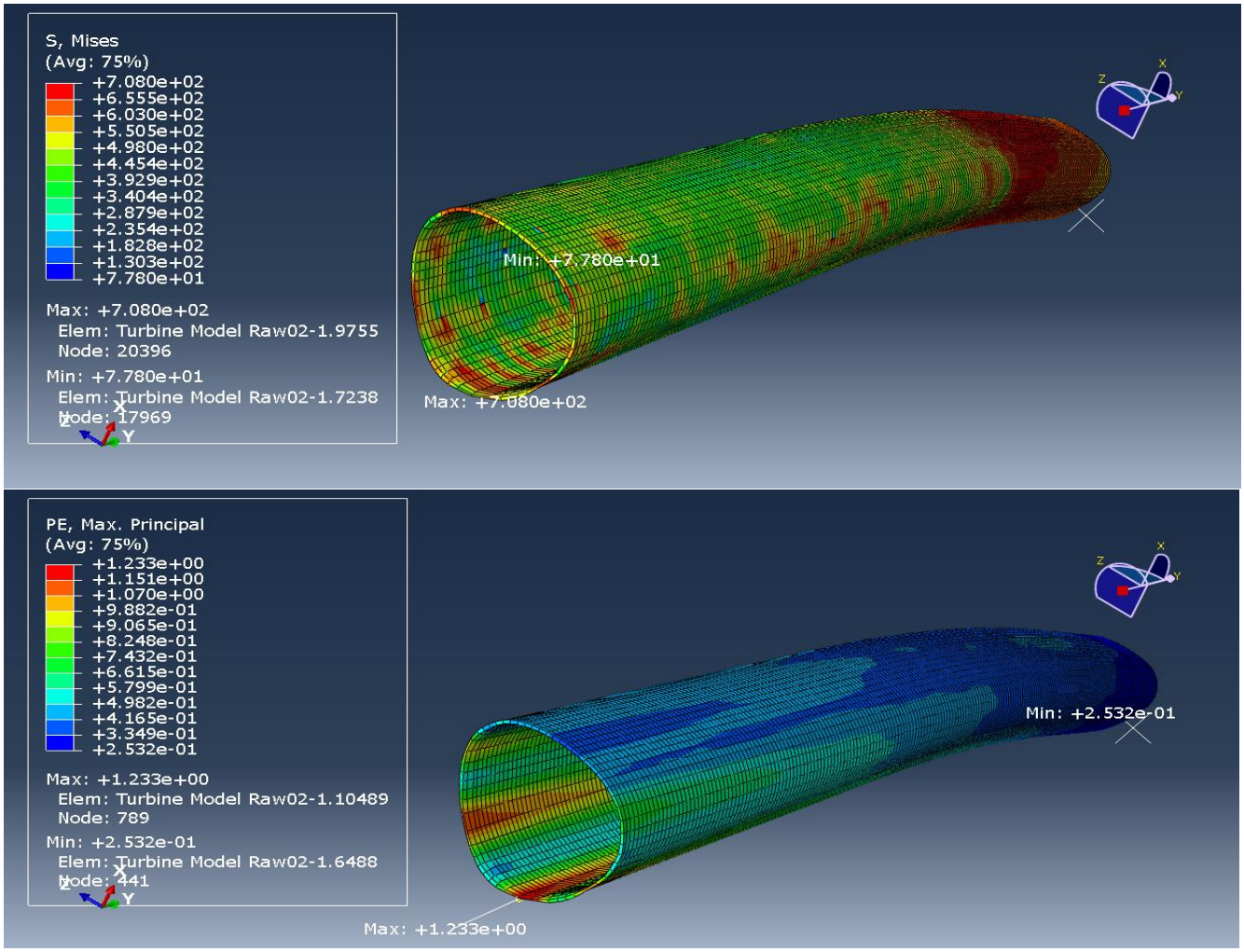

Figure 11. Position of the maximum and minimum stress contour

The maximum and minimum strain observed during forming are 1.23 and 2.53e-1 mm/mm. Figure 12 shows the diagram of strain demonstrated.

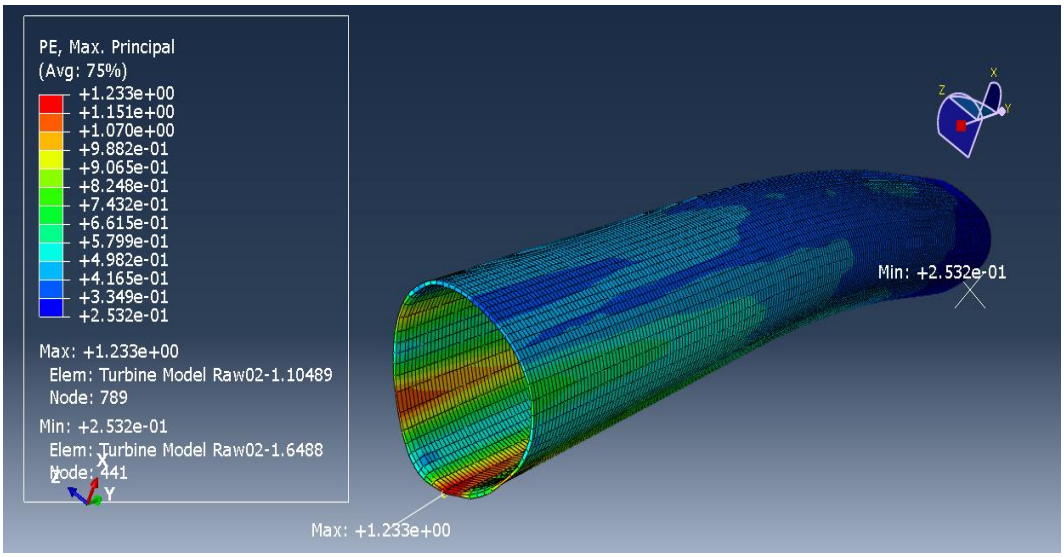

Figure 12. Diagram of strain

3.2 Thickness distribution

The wall thickness before and after forming respectively are 0.5mm and 0.37mm and it is approximately equal for all points around the specific contour. The wall thickness of the part before and after forming is shown in Figure 13. No sign of rupture was observed and it shows that the forming process is appropriately performed.

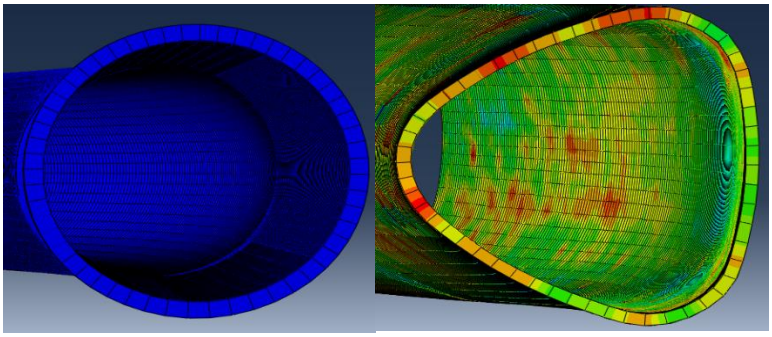

Figure 13. Wall thickness of part before and after forming

3.3 Stress in Die

The maximum Von Mises stress imposed on the die is equal to 425MPa and this occurs at the final stage of forming. This stress helps to select the appropriate steel alloy for the die. Figure 14 shows the stress imposed on the die.

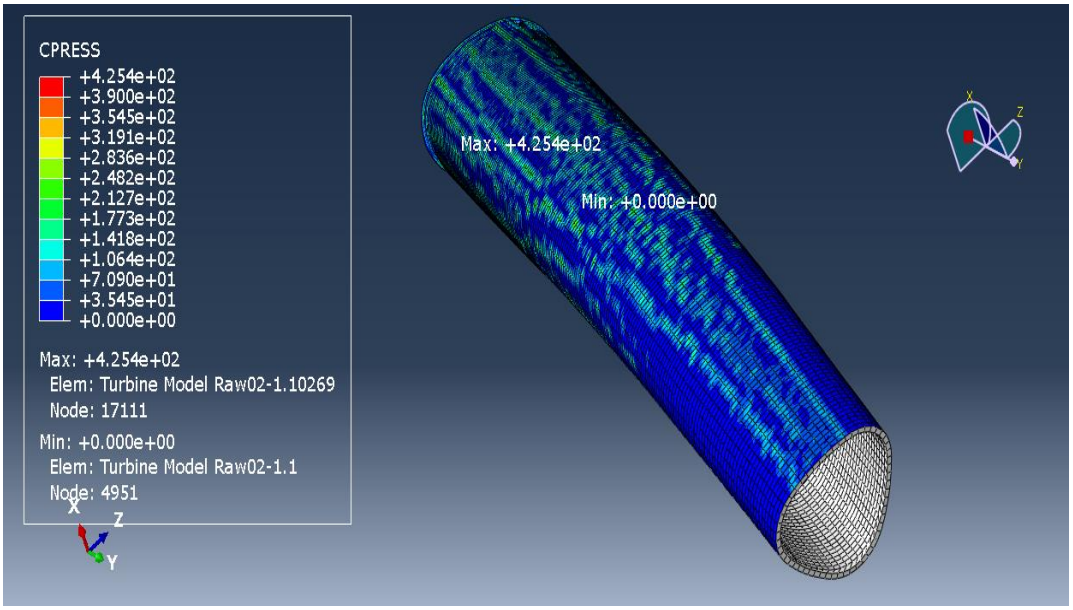

Figure 14. Stress imposing on the die

4. Conclusion

In this paper, the feasibility of manufacturing the dental drill body by hydroforming process was investigated. Due to hygienic issues the 304 stainless steel was selected, moreover, to make the integrated dental drill body with no seam weld, the hydroforming process was selected. The internal pressure was adjusted to obtain the final shape of the part. The initial part is completely formed according to the die geometry. In this forming process' simulation, no sign of rapture and waviness was observed. In addition, the wall thickness distribution (0.38mm) is approximately identical

through the final part. The maximum Von Misses stress that occurred in this simulation was equal to 708MPa and the maximum and minimum were 1.23 and 2.53e-1 mm/mm.

5. References

[1] Glenner, R.A. 1974. Development of the dental drill. The Journal of the American Dental Association. 88(4): 712-727.

[2] Zhang, J., Cheng, P., Wang, F., Tang, W. and Zhao, X. 2022. Hydroforming and buckling of an egg-shaped shell based on a petal-shaped preform. Ocean Engineering. 250: 111057.

[3] Liu, W., Chen, Y.-Z., Hu, L. and Zhang, Z.-C. 2022. Deformation of large curved shells using double-sided pressure sheet hydroforming process. International Journal of Lightweight Materials and Manufacture. 5(3): 397-410.

[4] Lei, Q., Li, M., Ilinich, A., Luckey, G. and Misra, A. 2019. Microstructural evolution and failure mechanism of an extrusion welded aluminum alloy tube during hydroforming processing. Materials Science and Engineering: A. 756: 346-353.

[5] Cui, X.-L. and Yuan, S.-J. 2019. Effects of superimposed hydrostatic pressure on bulging deformation and fracture of tubes in double-sided hydroforming. Archives of Civil and Mechanical Engineering. 19(2): 569-583.

[6] Mahdieh, M.S., Rafati, E. and Kargar Sichani, S. 2013. Investigation of variance of roller burnishing parameters on surface quality by taguchi approach. ADMT Journal. 6(3): 1-6.

[6] Jain, N. and Wang, J. 2005. Plastic instability in dual-pressure tube-hydroforming process. International Journal of Mechanical Sciences. 47(12): 1827-1837.

[7] Saraeian, P., Gholami, M., Behagh, A., Behagh, O., Javadinejad, H.R. and Mahdieh, M. 2016. Influence of vibratory finishing process by incorporating abrasive ceramics and glassy materials on surface roughness of ck45 steel. ADMT Journal. 9(4): 1-6.

[8] Vakili Sohrforozani, A., Farahnakian, M., Mahdieh, M.S., Behagh, A.M. and Behagh, O. 2019. A study of abrasive media effect on deburring in barrel finishing process. Journal of Modern Processes in Manufacturing and Production. 8(3): 27-39.

[9] Vakili Sohrforozani, A., Farahnakian, M., Mahdieh, M.S., Behagh, A.M. and Behagh, O. 2020. Effects of abrasive media on surface roughness in barrel finishing process. ADMT Journal. 13(3): 75-82.

[10] Mahdieh, M.S. 2020. The surface integrity of ultra-fine grain steel, electrical discharge machined using iso-pulse and resistance–capacitance-type generator. Proceedings of the Institution of Mechanical Engineers, Part L: Journal of Materials: Design and Applications. 234(4): 564-573.

[11] Mahdieh, M.S. 2020. Recast layer and heat-affected zone structure of ultra-fined grained low-carbon steel machined by electrical discharge machining. Proceedings of the Institution of Mechanical Engineers, Part B: Journal of Engineering Manufacture. 234(5): 933-944.

[12] Mahdieh, M.S. and Mahdavinejad, R. 2016. Comparative study on electrical discharge machining of ultrafine-grain al, cu, and steel. Metallurgical and Materials Transactions A. 47(12): 6237-6247.

[13] Mahdieh, M.S. and Zare-Reisabadi, S. 2019. Effects of electro-discharge machining process on ultra-fined grain copper. Proceedings of the Institution of Mechanical Engineers, Part C: Journal of Mechanical Engineering Science. 233(15): 5341-5349.

[14] Mahdieh, M.S. and Mahdavinejad, R.A. 2017. A study of stored energy in ultra-fined grained aluminum machined by electrical discharge machining. Proceedings of the Institution of Mechanical Engineers, Part C: Journal of Mechanical Engineering Science. 231(23): 4470-4478.

[15] Mahdieh, M.S. and Mahdavinejad, R. 2018. Recast layer and micro-cracks in electrical discharge machining of ultra-fine-grained aluminum. Proceedings of the Institution of Mechanical Engineers, Part B: Journal of Engineering Manufacture. 232(3): 428-437.

[16] Jain, N. and Wang, J. 2005. Plastic instability in dual-pressure tube-hydroforming process. International Journal of Mechanical Sciences. 47(12): 1827-1837.

[17] Mapar, A., Bieler, T., Pourboghrat, F., Compton, C. and Murphy, J. 2015. Hydroforming of large grain niobium tube. 17th International Conference on RF Superconductivity.

[18] Raut, S.V., Ramesh, A., Arun, A. and Sumesh, C. 2021. Finite element analysis and optimization of tube hydroforming process. Materials Today: Proceedings. 46: 5008-5016.

[19] Ma, J., Yang, L., Huang, J., Chen, Z., He, Y. and Jiang, J. 2021. Residual contact pressure and elastic recovery of an assembled camshaft using tube hydroforming. CIRP Journal of Manufacturing Science and Technology. 32: 287-298.

[20] Zhang, Z., Kang, Y., Furushima, T., Manabe, K.-i., Wang, C. and Li, B. 2020. Deformation behaviour of metal micro tube during hydroforming process. Procedia Manufacturing. 50: 328-331.

[21] Jiao, Z.-h., Lang, L.-h. and Zhao, X.-n. 2021. 5a06-o aluminium–magnesium alloy sheet warm hydroforming and optimization of process parameters. Transactions of Nonferrous Metals Society of China. 31(10): 2939-2948.

[22] Zaheer, O., Ingarao, G., Di Lorenzo, R. and Fratini, L. 2021. On the effectiveness of spif process to re-form end-of-life components as compared to conventional forming approach. Key Engineering Materials. 883: 201-208.

[23] Han, S., Woo, Y., Hwang, T., Oh, I. and Moon, Y.H. 2019. Tailor layered tube hydroforming for fabricating tubular parts with dissimilar thickness. International Journal of Machine Tools and Manufacture. 138: 51-65.

[24] Novotny, S. and Geiger, M. 2003. Process design for hydroforming of lightweight metal sheets at elevated temperatures. Journal of Materials Processing Technology. 138(1-3): 594-599.

[25] Kocańda, A. and Sadłowska, H. 2008. Automotive component development by means of hydroforming. Archives of Civil and Mechanical Engineering. 8(3): 55-72.

[26] Ahmetoglu, M. and Altan, T. 2000. Tube hydroforming: State-of-the-art and future trends. Journal of Materials Processing Technology. 98(1): 25-33.

[27] Desu, R.K., Krishnamurthy, H.N., Balu, A., Gupta, A.K. and Singh, S.K. 2016. Mechanical properties of austenitic stainless steel 304l and 316l at elevated temperatures. Journal of Materials Research and Technology. 5(1): 13-20.

[28] Gheisary, M. and Djavanroodi, F. 2010. Experimental and numerical investigation of double bulge tube hydroforming. Modares Mechanical Engineering. 10(3): 1-9.

[29] Hwang, Y.-M. and Altan, T. 2003. Finite element analysis of tube hydroforming processes in a rectangular die. Finite Elements in Analysis and Design. 39(11): 1071-1082.

[30] Hwang, Y.-M. and Lin, Y.-K. 2002. Analysis and finite element simulation of the tube bulge hydroforming process. Journal of materials processing technology. 125: 821-825.

[31] Zadeh, H.K. and Mashhadi, M.M. 2006. Finite element simulation and experiment in tube hydroforming of unequal t shapes. Journal of Materials Processing Technology. 177(1-3): 684-687.

[32] Khorsandi, A. and Loh-Mousavi, M. 2010. Numerical investigations on the effect of pulsating pressure on improvement of formability in hydroforming of bent tube by fem. Journal of Simulation and Analysis of Novel Technologies in Mechanical Engineering. 3(1): 11-20.

[33] Choi, H.-H., Hwang, S.-M., Kang, Y., Kim, J. and Kang, B. 2002. Comparison of implicit and explicit finite-element methods for the hydroforming process of an automobile lower arm. The International Journal of Advanced Manufacturing Technology. 20(6): 407-413.

[34] Loh-Mousavi, M., Bakhshi-Jooybari, M., Mori, K., Farzin, M., Hosseinipour, J. 2010. Experimental study and numerical study of pulsating hydroforming of tube in box-shaped die. 21(1): 47-58.

[35] Mohammadalizade, F., Gorji, A., Bakhshi, M. and Elyasi, M. 2016. Reforming internal pressure and axial feeding loading paths in hydroforming process of cylindrical stepped tube in order to improve the thickness distribution. Amirkabir Journal of Mechanical Engineering. 48(4): 389-400.